THE SEISMOLOGICAL SOCIETY OF AMERICA
400 Evelyn Ave., Suite 201
Albany, CA 94706-1375
(510) 525-5474; FAX (510) 525-7204
www.seismosoc.org

Bulletin of the Seismological Society of America, Vol. 106, No. 4, pp. –, August 2016, doi: 10.1785/0120150367

Ⓔ

Region-Specific Assessment, Adjustment, and Weighting of Ground-Motion Prediction Models: Application to the 2015 Swiss Seismic-Hazard Maps

by Benjamin Edwards, Carlo Cauzzi, Laurentiu Danciu, and Donat Fäh

Abstract We present a strategy for the region-specific assessment, adjustment, and weighting of ground-motion prediction models, with application to the 2015 Swiss national seismic-hazard maps. The models are provided within a logic-tree framework adopted for the probabilistic seismic-hazard analysis (PSHA). Through this framework, we consider both aleatory and epistemic uncertainties in ground-motion prediction in Switzerland, a region of low-to-moderate seismicity and consequently data poor in terms of strong-motion records. We use both empirical models developed using global strong-motion data and stochastic simulation models calibrated to local seismicity, characteristic wave-propagation effects, and site conditions. The empirical models were adjusted to account for (a) the selected hazard reference rock velocity model (using V_S–κ_0 adjustments) and (b) the median instrumental ground-motion data at low magnitudes. The use of a carefully calibrated simulation model and V_S–κ_0 adjusted empirical ground-motion prediction equations allowed us to precisely define the reference-rock profile, upon which subsequent analyses, such as microzonation and site-specific hazard, can be applied without uncertainty related to the reference condition. We implemented partially nonergodic aleatory uncertainties in ground-motion prediction through the single-station sigma approach. This strategy, complemented with the known reference rock condition, leads to significant reductions in the contribution of uncertainty in ground-motion characterization to PSHA in Switzerland. However, the application of the methodological framework outlined herein extends to any region, particularly those of low-to-moderate seismicity.

Online Material: Tables of adjustment factors to convert selected ground-motion prediction equations (GMPEs) to the Swiss rock reference and figures showing trellis plots of all adjusted GMPEs with uncertainty estimates.

Introduction

Lying between the seismically active region of Italy to the south and the low-seismicity regions of northern Europe, earthquake activity in Switzerland can be described as moderate (Giardini *et al.*, 2014). Over the entire region, earthquakes with moment magnitude M_w 5 are expected approximately every 10 years and M_w 6 every 100 years. The most recent significant event, with M_w 5.8 (Earthquake Catalogue of Switzerland [ECOS09]; Fäh *et al.*, 2011), occurred in Sierre, Canton Valais, on 25 January 1946. The epicentral intensity reached degree VIII on the European Macroseismic Scale 1998 (EMS-98), corresponding to moderate-to-significant damage within a radius of about 25 km. A strong aftershock ($M_w \sim 5.5$) with significant secondary effects (landslides, rockfalls, etc.) followed closely afterward on 30 May. This is by no means unusual for the region of Valais, which dominates the national seismic hazard (Wiemer *et al.*, 2009), with significant events (around M_w 6 or greater) having occurred in 1524, 1584, 1685, 1755, 1855, and 1946 (Fritsche and Fäh, 2009). The strongest documented earthquake (M_w 6.6, EMS-98 epicentral intensity IX) to have occurred in central Europe was located in the region of Basel (at the border with Switzerland, France, and Germany) in 1356, with significant destruction to the city (Fäh *et al.*, 2009).

Based on well-documented historical seismicity in Switzerland (Gisler *et al.*, 2003, 2007; Schwarz-Zanetti *et al.*, 2003, 2004; Gisler, Fäh, and Deichmann, 2004; Gisler, Fäh,

and Kastli, 2004; Gisler, Fäh, and Schibler, 2004; Fritsche *et al.*, 2006; Fäh *et al.*, 2009; Fritsche *et al.*, 2009, 2012), seismic hazard is clearly an important issue to address. The topic has seen significant focus and progress in the last 15 years. Between 2000 and 2004, a multinational research project (probabilistic seismic-hazard analysis for Swiss Nuclear Power Plant Sites [PEGASOS]) was undertaken by swissnuclear, the nuclear energy section of the swisselectric group (Abrahamson *et al.*, 2002). In parallel, the Swiss Seismological Service (SED) undertook a national seismic-hazard assessment (Wiemer *et al.*, 2009), leading to the previous national seismic-hazard map that was delivered in 2004. In follow-up to the PEGASOS project, swissnuclear undertook a Senior Seismic Hazard Analysis Committee (SSHAC) Level 4 seismic-hazard assessment project (PEGASOS Refinement) from 2008 to 2014 (Renault, 2014). On a wider scale, the European Union project Seismic Hazard Harmonization in Europe (SHARE), which began in 2009, resulted in Europe-wide seismic-hazard maps, published in 2013 (Woessner *et al.*, 2015).

This article forms part of the scientific documentation of the most recent assessment of the national seismic hazard by the SED, with the final national seismic-hazard maps delivered in 2015 (see Data and Resources). The national seismic hazard is assessed using the probabilistic approach originally developed by Cornell (1968). This approach integrates possible earthquake sources and their resulting ground-motion fields over time. This article focuses on the latter component, that is, the definition of ground-motion fields for prescribed earthquake sources. However, a brief summary of the earthquake source model used as input to the 2015 Swiss seismic-hazard maps is given here for completeness. The earthquake source model combines four components: the original area source model of the 2004 Swiss Hazard Model (Giardini *et al.*, 2004), the relevant area sources of the 2013 SHARE model (Woessner *et al.*, 2015), an updated version of the 2004 area sources, and a newly developed smoothed-seismicity model conceptually similar to that presented by Hiemer *et al.* (2014). The first two models were inherited entirely without modification from the original seismic source models. The latter two are newly developed to reflect the latest seismicity observations and harmonization of the earthquake catalog (ECOS-09, Fäh *et al.*, 2011). A penalized maximum-likelihood method was used for recurrence-rate parameter estimation and the Electric Power Research Institute approach for estimating the maximum magnitude, as described by Johnston *et al.* (1994) and Hiemer *et al.* (2014). The four seismic source models are weighted per magnitude bins in an ensemble earthquake-rate forecast. Each model is characterized by a recurrence-rate distribution for each magnitude, and five branches are sampled to represent the uncertainties of the earthquake recurrence rates for each magnitude bin. The five earthquake rate branches (Fig. 1) are spatially distributed over a grid of point sources that cover Switzerland and border regions. The resulting earthquake scenarios, accounting for uncertainties of seismicity patterns, for earthquake completeness in time and space, for style of faulting, for seismicity depth-distribution, for maximum magnitude, and for earthquake recurrence parameters are then used as input to the ground-motion prediction equations (GMPEs) to estimate probabilities of exceedance for different ground-motion levels.

The prediction of earthquake ground motions is nontrivial due to the complex nature of earthquake sources and wave propagation through complex media. Although deterministic models using either kinematic or dynamic rupture representations are produced for well-studied earthquakes and/or active faults (e.g., Dalguer *et al.*, 2008; Graves and Pitarka, 2010), the significant uncertainty of input parameters for future earthquakes means that simplifications and assumptions have to be made. In practice, this is done through the development of GMPEs, which act as a statistical tool to provide the expected mean and standard deviation of (logarithmically transformed) ground motions for a given set of simplified earthquake descriptors (predictors, explanatory variables). The main predictor variables in current GMPEs are earthquake magnitude, a measure of source-to-site distance, style of faulting (i.e., normal, reverse, or strike slip), and one or more terms to describe the local site classification (upper 30 m time-averaged shear-wave velocity, depth to bedrock, etc.). GMPEs are calibrated based on either empirical data or simulated data. Different authors have developed models for global mixtures of events (e.g., the Next Generation Attenuation (NGA) database, Chiou *et al.*, 2008), for only regional events (e.g., the European and Middle East database, Akkar *et al.*, 2014), or for only local events (e.g., the Japanese database, Zhao *et al.*, 2006). Differences in GMPEs arise from using different datasets, raising an open question as to the regional effects on ground motion (Stafford, 2014).

GMPE Selection

Despite the recent development of a modern and dense seismic network (Clinton *et al.*, 2011; Cauzzi and Clinton, 2013; Diehl *et al.*, 2013, 2014; Michel *et al.*, 2014), the availability of GMPEs specifically developed for Switzerland is significantly limited, due to a recent quiescence in seismicity. In fact, the largest events recorded on modern instrumentation have all occurred outside Swiss borders, for example, the St. Dié, France, earthquake with M_L 5.3 (M_w 4.6); the 1999 Bormio, Italy, event with M_L 4.9 (M_w 4.9); and the 2004 Garda, Italy, event with M_L 5.0 (M_w 5.0). The largest event to have recently occurred within Swiss borders was the 1991 Vaz earthquake with M_L 5.0 (M_w 4.7). This lack of strong-motion data leaves two main options for the development of regional GMPEs: the use of data from other, more seismically active regions of the world or the simulation of ground-motion data.

Availability and Selection of Empirical Models

Because of the high number of available GMPEs developed around the world, strict selection criteria are often used to limit our choice to the required number of models

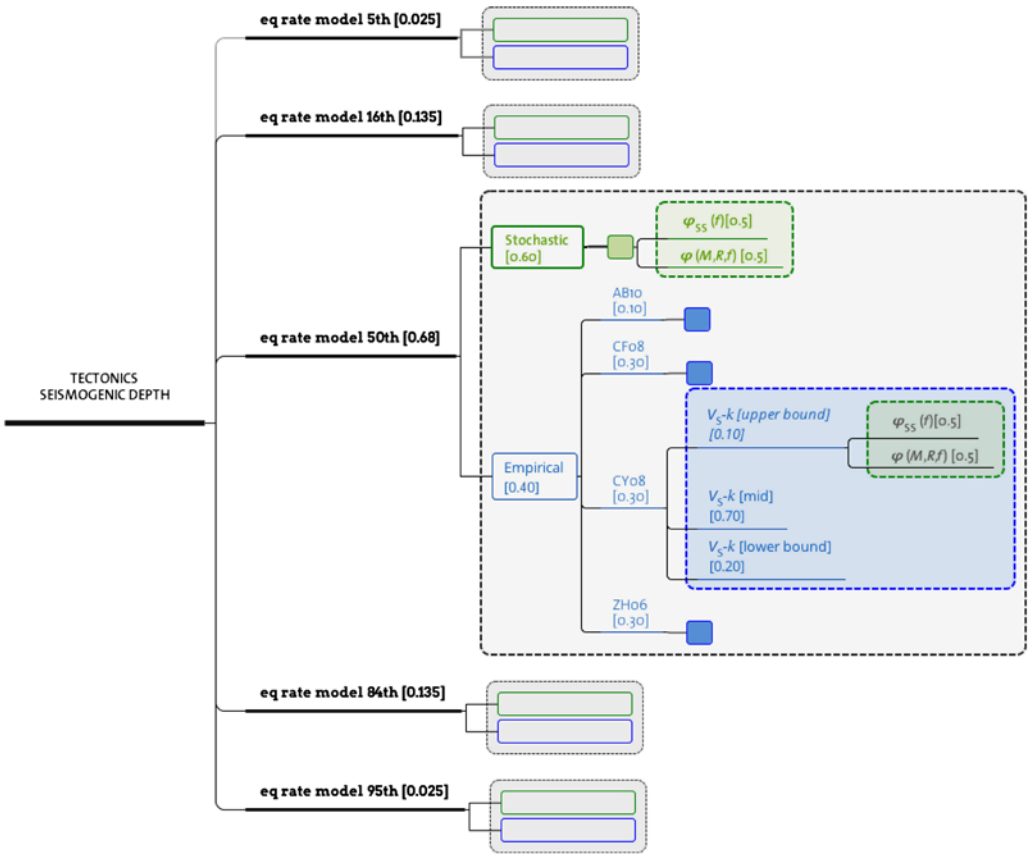

Figure 1. Master logic tree depicting the earthquake-rate forecast models and the ground-motion models. Empty branches indicate a repetition of the ground-motion branches (stochastic and empirical). Abbreviations are described in the text. The color version of this figure is available only in the electronic edition.

(Bommer *et al.*, 2010). Previous GMPEs selected for use in Switzerland in the recent SHARE project and the two PEGASOS projects are given in Table 1. The SHARE project segregated Switzerland into two broad tectonic regions, stable continental to the north and shallow active to the south. Such a distinction is strongly debated; however, the GMPEs used for the two regions present a great deal of overlap (Table 1).

Since the end of the SHARE and PEGASOS probabilistic seismic-hazard analysis (PSHA) projects, and during the course of the current national seismic-hazard project, several high-quality new GMPEs became available, notably the NGA-West2 dataset-based models (Ancheta *et al.*, 2014; Gregor *et al.*, 2014), the European and Middle East Reference database for seismic ground-motion in Europe (RESORCE) dataset-based models (Akkar *et al.*, 2014; Douglas *et al.*, 2014), and a major update of the broadband prediction model of the Cauzzi and Faccioli (2008) GMPE (Cauzzi, Faccioli, *et al.*, 2015). Despite the availability of these equations arising during the current project, which began in 2013, it was decided not to implement them. The reason for this was primarily due to the fact that significant testing and verification had been carried out on the existing GMPEs over the course of other recent hazard projects. This was not the case for the newly published equations; errata to any of the models would prove extremely costly due to the numerous stages of conversion required for implementation in Switzerland. Based on GMPE implementation and testing in previous projects, we therefore decided to select the following four empirical GMPEs: Akkar and Bommer (2010), Chiou and Youngs (2008), Cauzzi and Faccioli (2008), and Zhao *et al.* (2006); hereinafter the models are referred to as AB10, CY08, CF08, and ZETAL06, respectively (Table 1). The chosen predictive models are the same used in project SHARE for regions with active shallow crustal seismicity. AB10 is generally considered to be representative of Euro-Mediterranean seismicity, because it is based on data from the European and Middle East strong ground motion database (Ambraseys *et al.*, 2004). A significant limitation of this model is the use of simple site classification (rock, stiff soil, soft soil, very soft soil), which introduces large uncertainties if site amplification and attenuation adjustments are implemented. Despite being based on worldwide data (the NGA database) with primarily Californian events for moderate magnitudes, CY08 was found to be suitable for ground-motion prediction in the greater European region by Delavaud *et al.* (2012). CY08 uses a more sophisticated ground-type classification based on V_{S30}, making host-to-site adjustments somewhat easier. V_{S30} is also used by CF08, a global model

Table 1
Overview of GMPEs Used in Recent Seismic-Hazard Projects in Switzerland

	SHARE (Stable Continental Regions)	SHARE (Active Shallow Crustal Regions)	PEGASOS Refinement	Swiss Hazard 2014	References
AB06 *			‡		Atkinson and Boore (2006)
AB10	†	†	†	†	Akkar and Bommer (2010)
AC10			†		Akkar and Cagnan (2010)
AS08			†		Abrahamson and Silva (2008)
BA08			†		Boore and Atkinson (2008)
BETAL11			‡		Bindi *et al.* (2011)
CA03 *	†				Campbell (2003)
CB08			†		Campbell and Bozorgnia (2008)
CF08	†	†		†	Cauzzi and Faccioli (2008)
CY08	†	†	†	†	Chiou and Youngs (2008)
TO02 *	†		‡		Toro *et al.* (1997)
ZETAL06		†	†	†	Zhao *et al.* (2006)
EF13 *			†	†	Edwards and Fäh (2013b)

SHARE, Seismic Hazard Harmonization in Europe; PEGASOS, probabilistic seismic-hazard analysis for Swiss Nuclear Power Plant sites.
*Simulation-based models
†Ground-motion prediction equations (GMPEs) that were used.
‡GMPEs that were evaluated but not used.

dominated by Japanese data, with a significant contribution from Italian data at small-to-moderate magnitudes. CF08 is notable in its use of only digital recordings and a careful characterization of the geophysical properties of the recording sites. ZETAL06 uses exclusively Japanese data, with site classification based on natural period. A comprehensive overview of the functional forms, prediction variables, and recommended magnitude and distance application ranges for the above-mentioned empirical GMPEs is given in Douglas (2015) (see Data and Resources).

Cua and Heaton (2008) developed a model for predicting peak ground acceleration (PGA) and peak ground velocity (PGV) by combining weak-motion recordings from Switzerland with strong-motion recordings from the NGA (Power *et al.*, 2008) database (Chiou *et al.*, 2008). The Cua and Heaton (2008) equations have been the basis for the ShakeMap (Worden *et al.*, 2010) implementation at the Swiss Seismological Service until their recent revision in 2014 (Cauzzi, Edwards, *et al.*, 2015). The model is, however, not used in the Swiss national seismic-hazard assessment because it does not cover response spectral ordinates (elastic 5% damped pseudospectral acceleration [PSA]) over a broad vibration period range, which will form the basis of the hazard analyses.

Available Simulation-Based Models

To overcome the issue of limited strong-motion data in Switzerland, Bay *et al.* (2005) built on their earlier work (Bay *et al.*, 2003) by implementing the stochastic point-source ground-motion simulation method, as described in detail by Boore (2003). The stochastic simulation approach and related random vibration theory (RVT) techniques (e.g., Cartwright and Longuet-Higgins, 1956; Hanks and Mcguire, 1981) rely on the observation that high-frequency earthquake acceleration time series can be approximated by duration-limited random-phase signal, with frequency content modulated by a simple representation of the earthquake source, path, and site effects. The synthetic GMPE of Bay *et al.* (2005) was used for the 2004 Swiss national hazard maps (Wiemer *et al.*, 2009), providing predictions at vibration frequencies between 1 and 15 Hz.

A significant issue related to point-source models is their applicability for larger earthquakes, in which finite ruptures tend to spread the radiated energy over a wider source region. Point-source simulation models therefore significantly overestimate ground motions from large earthquakes in the near-field region. Recent improvements to stochastic simulation methods have introduced either finite sources composed of numerous subfaults (Motazedian and Atkinson, 2005) or geometrical effects to account for near-source saturation effects (Atkinson and Silva, 2000; Rietbrock *et al.*, 2013). Although the subfault solution is more flexible, it also requires more input parameters, including knowledge of the hypocenter location. For the purposes of ground-motion prediction in Switzerland, this is not known *a priori*. In contrast, Boore (2009) showed that for randomized hypocenter locations, the so-called effective distance measure (R_{EFF}), in practice a geometrical adjustment, produces saturation effects (which are magnitude-, distance-, and period-dependent) comparable to subfault models and to the observations of real earthquakes.

With this background, Edwards and Fäh (2013b) developed a stochastic ground-motion simulation model for Switzerland based on their and others' earlier work characterizing attenuation (Edwards *et al.*, 2011) and crustal amplification (Poggi *et al.*, 2011) in the greater Swiss region. The model was based on the spectral analysis of Swiss earthquakes recorded on the broadband seismic network and was calibrated at high magnitudes to historical macroseismic observations (Fäh *et al.*, 2011). Their model provides elastic 5% damped

PSA at vibration periods between PGA (0 s and 2 s), and PGV. The predictions are for a well-defined reference-rock profile (Poggi *et al.*, 2011), with differentiation between foreland and alpine motions. The use of a reference rock velocity profile marked a significant improvement on previous empirical and simulation-based models, which left the reference-rock profile unknown (only defined, for example, by a site class or V_{S30} range). The model of Edwards and Fäh (2013b) for the Swiss foreland was used in the PEGASOS Refinement project and has recently been integrated into the ShakeMap implementation at the SED (Cauzzi, Edwards, *et al.*, 2015) through parameterization into a functional form, allowing its implementation into the OpenQuake hazard engine (Silva *et al.*, 2014). As part of the comprehensive quality-assurance process, the model was tested against free-field surface accelerometer data from Japan using KiK-net (strong-motion seismographs installed in a borehole and on the ground surface), and it was found to provide, after adjustment for regional effects, predictions comparable with existing GMPEs for the region for magnitudes up to M_w 7. For this project, we therefore implement the parameterized version (Cauzzi, Edwards, *et al.*, 2015) of the model of Edwards and Fäh (2013b). The regional components (alpine and foreland) are used; however, rather than the fixed stress parameter of 6 MPa suggested by Edwards and Fäh (2013b), we use a variable-source stress parameter to account for epistemic uncertainty in the model (e.g., Douglas *et al.*, 2013; Edwards and Douglas, 2013; Bommer *et al.*, 2016). This is calibrated based on testing against macroseismic intensity data points (as discussed in Cauzzi, Edwards, *et al.*, 2015). The previously developed model by Bay *et al.* (2005), as implemented in the previous national seismic-hazard maps, is not used due to the fact that it is entirely point-source based and therefore does not provide reasonable predictions in the near field of large earthquakes, nor does it refer to a well-constrained velocity profile.

Empirical GMPEs: Calibration and Adjustment

Following the approaches of the SHARE and PEGASOS Refinement projects, the selected empirical GMPEs were adjusted to account for Swiss rock reference conditions and extension to smaller magnitudes.

V_S–κ_0 Adjustments

Two principal elements make up the site component of ground-motion predictions as input to PSHA: elastic amplification and near-surface site-specific attenuation. Elastic amplification, and to some extent the associated attenuation, can be considered a direct consequence of the local velocity profile beneath the site. Nonlinearity (e.g., soil plasticity) also plays a role at high levels of shaking at particular soil sites. However, this is generally assumed to be regionally independent (i.e., a property only of the soil, and therefore V_{S30}) and described either implicitly or explicitly by individual GMPEs. Also, nonlinearity is of comparably lesser importance for shaking predictions at rock sites.

Kappa (κ) controls the high-frequency decay of the Fourier amplitude spectrum (FAS) of earthquake ground motion (Anderson and Hough, 1984) and has a significant impact on the results of PHSA at high vibration frequencies (Renault, 2014). Its site-specific zero-distance component (κ_0) represents the attenuation of shear waves below and near a given site due to the mechanical and geophysical properties of the subsurface geomaterials. The host-to-target adjustment, often referred to as V_S–κ_0 adjustment, aims at mapping changes in the velocity profiles from the host region (implicitly defined in the GMPE) to the target region: in this case, Switzerland.

The target velocity profile forms part of the definition of the hazard model. In this study, we use the velocity model of Poggi *et al.* (2011) and associated amplification. By design, therefore, there is no epistemic uncertainty associated with the reference-rock profile in the target region. Epistemic uncertainty in the near-surface attenuation for this reference velocity profile is considered to be captured by the alternative use of (a) the model by Anderson and Hough (1984) with $\kappa_0 = 0.0159$ s (Edwards *et al.*, 2011) and (b) $\kappa_0 = 0.0260$ s (Poggi *et al.*, 2013), the former being consistent with the simulation model of Edwards and Fäh (2013b).

We employ a systematic approach to account for the differences in host (GMPE-based) velocity profiles, as detailed in Al Atik *et al.* (2014). This approach has the advantage that, unlike other approaches for determining κ_0 from response spectra, no assumption of the background seismological model (e.g., Q, $\Delta\sigma$, etc.) is required. Frequency-dependent adjustment functions $C_{\mathrm{FAS},V_S-\kappa_0}$ are initially determined based on the ratio of the predicted FAS at rock reference sites in the host and target region for a given scenario

$$C_{\mathrm{FAS},V_S-\kappa_0}(f) = \frac{A_{\mathrm{target}}(f)}{A_{\mathrm{host}}(f)} e^{-\pi f(\kappa_{0,\mathrm{target}}-\kappa_{0,\mathrm{host}})} \approx \frac{\mathrm{FAS}_{\mathrm{target}}}{\mathrm{FAS}_{\mathrm{GMPE}}}(f), \quad (1)$$

in which A describes amplification and κ_0 describes attenuation in the GMPE (host) and target regions. Using the host and target velocity profiles, amplification A was determined through 1D-*SH* wave propagation for both the GMPE and target regions (Knopoff, 1964). Because the chosen predictive models provide only response spectra and peak ground motions, response spectrum compatible $\mathrm{FAS}_{\mathrm{GMPE}}$ was obtained through inverse RVT (iRVT) (Rathje *et al.*, 2005) using the computer program Strata (Kottke and Rathje, 2008). The iRVT method takes the input GMPE response spectrum ($\mathrm{PSA}_{\mathrm{GMPE}}$) and provides a best-fit spectrum ($\mathrm{PSA}_{\mathrm{GMPE,iRVT}}$) and the corresponding FAS ($\mathrm{FAS}_{\mathrm{GMPE}}$). $\mathrm{FAS}_{\mathrm{GMPE}}$ is then directly adjusted using $C_{\mathrm{FAS},V_S-\kappa 0}$ (equation 1), which is calculated based on A and κ_0, before being restored to the response spectral domain ($\mathrm{PSA}_{\mathrm{target}}$) through RVT. The PSA-based adjustment can then be defined as

$$C_{\mathrm{PSA},V_S-\kappa_0}(T) = \frac{\mathrm{PSA}_{\mathrm{target}}}{\mathrm{PSA}_{\mathrm{GMPE,iRVT}}}(T), \qquad (2)$$

which is averaged over different scenarios and can be used to directly adjust GMPEs for prediction at the target site. Initially, we used nine scenarios (M_w 4, 5, 6; and R_{JB} = 5, 10, 20 km); however, we found that there was limited sensitivity to the selected scenario, and therefore used a single scenario to define $C_{\mathrm{PSA},V_S-\kappa_0}$. Although Al Atik *et al.* (2014) suggest using $\mathrm{PSA}_{\mathrm{GMPE}}$ directly in equation (2), we found that the $\mathrm{PSA}_{\mathrm{GMPE}}$ could not always be matched with $\mathrm{PSA}_{\mathrm{GMPE,iRVT}}$. In our implementation, we therefore use $\mathrm{PSA}_{\mathrm{GMPE,iRVT}}$ to define the final PSA-based adjustment factors. As a cross-check, we found that this approach is consistent with that of Campbell (2003), which uses GMPE compatible stochastic models to make the adjustment to the response spectrum. We detail, here, the $V_S-\kappa_0$ adjustment procedure for CY08, whereas the adjustments operated on the other empirical models are given in Ⓔ Tables S1–S4 (available in the electronic supplement to this article). The host and target parameters defining A and κ_0 are as follows:

1. our target V_S profile for Swiss rock sites is always that of Poggi *et al.* (2011);
2. the V_S profile of CY08 in our study is either that of Boore and Joyner (1997) or an adjusted version of Poggi *et al.* (2011), both with V_{S30} = 620 ms^{-1} (Fig. 2);
3. κ_0 at rock sites in the host region (western United States) is estimated either based on Edwards *et al.* (2011), with κ_0 = 0.0218 s; Poggi *et al.* (2013), with κ_0 = 0.0345 s; or the iRVT technique, 0.0356 s;
4. κ_0 at hard rock sites in the target region (Switzerland) is estimated either based on Edwards *et al.* (2011), with κ_0 = 0.0159, or Poggi *et al.* (2013) with κ_0 = 0.0260.

Items (2)–(4) are designed to capture the epistemic uncertainty associated with assessing κ_0 in Switzerland and in the western United States, and defining the reference V_S profile at rock sites in the western United States. The host V_S profile for CH08 is based on Boore and Joyner (1997) because the majority of data used for the GMPE are from recording stations in the western United States and California. For predictions in the host region, we used a V_{S30} = 620 ms^{-1}, corresponding to the majority of the rock sites in Boore and Joyner (1997). This was assessed as part of the SSHAC Level 4 PEGASOS Refinement Project and largely based on personal communications with the authors of the predictive model. To cover the epistemic uncertainty related to this selection, we also used another generic-rock profile, namely that of Poggi *et al.* (2011), adjusted to V_{S30} = 620 ms^{-1}.

Several methods can be used to define κ_0. One option is to use the value determined from directly fitting the $\mathrm{FAS}_{\mathrm{GMPE}}$ from the iRVT approach described above. Alternatively, one can use empirical relations between V_{S30} and κ_0 (e.g., Silva *et al.*, 1998; Chandler *et al.*, 2006; Edwards and Fäh, 2013a) to define κ_0 or, alternatively, to directly define $\Delta\kappa_0 = \kappa_{0,\mathrm{target}} - \kappa_{0,\mathrm{host}}$, accounting for the host–target conversion. The latter approach, defining $\Delta\kappa_0$, avoids mixing different $V_{S30}-\kappa_0$ relations, which may have methodological (Edwards *et al.*, 2015) or regional biases, and instead shows the expected change due to the host-to-target conversion. Using the iRVT approach means including a directly measured estimate for the host, which may be more reliable than $V_{S30}-\kappa_0$ relations. Without mixing different $V_{S30}-\kappa_0$ relations, (c) and (d) yield four different values of $\Delta\kappa_0$, as listed in Table 2. Both the iRVT- and $V_{S30}-\kappa_0$-based $\Delta\kappa_0$ approaches are independent of background seismological models, which would be required if performing a full host-to-target conversion (Campbell, 2003; Scherbaum *et al.*, 2006).

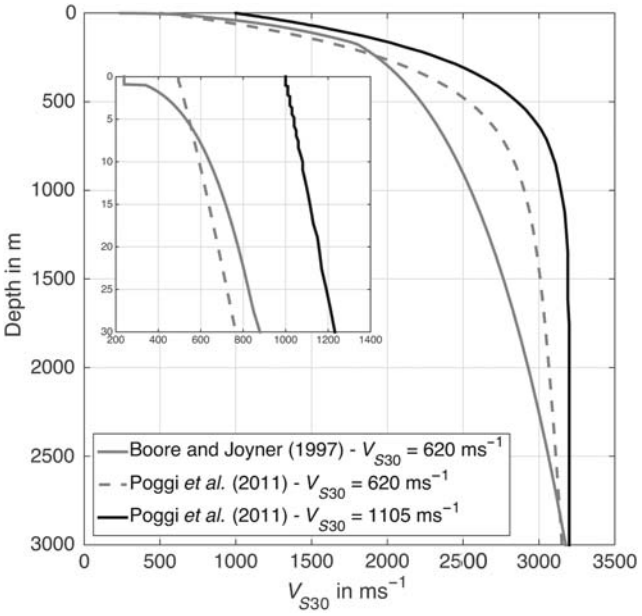

Figure 2. Host rock V_S profiles used for adjusting the Chiou and Youngs (2008; referred as CY08) ground-motion prediction equations (GMPE), as described in the text. The onset shows the V_S profiles in the uppermost 30 m.

The resulting suite of $V_{S30}-\kappa_0$ adjustments (eight in total, based on two amplification functions and four $\Delta\kappa_0$ values) is shown by the shaded area in Figure 3 for CY08. Among all the possible adjustments, only three, representative of the mean, lower- and upper-bound adjustments were retained to build the PSHA logic tree to avoid too many branches. The adjustments are implemented as period-dependent multiplicative factors ($C_{\mathrm{PSA},V_S-\kappa_0}(T)$) to be applied to the original GMPEs. For vibration periods $T > 0.2$ s, the adjustments result in a decrease of the original spectral levels, irrespective of the V_S profile and $\Delta\kappa_0$ values.

Small Magnitude Adjustments

Empirical GMPEs are often derived from datasets with moderate-to-large events, typically with M_w larger than ~5, mainly because such events are likely to cause damage to the built environment and are therefore of primary interest for engineering applications. Additionally, the metadata (magnitude, depth, distance to fault, etc.) for moderate and larger events are reasonably well known. For smaller events this

Table 2
Host and Target κ_0 along with $\Delta\kappa_0$ Used to Adjust CY08 to Swiss Rock Conditions

Source		Values		
Host κ_0	Target κ_0	Host κ_0	Target κ_0	$\Delta\kappa_0$
EETAL11	EETAL11	0.0218	0.0159	−0.0059
PETAL13	PETAL13	0.0345	0.0260	−0.0085
iRVT	EETAL11	0.0365	0.0159	−0.0206
iRVT	PETAL13	0.0365	0.0260	−0.0105

CY08, Chiou and Youngs (2008); EETAL11, Edwards *et al.* (2011); PETAL13, Poggi *et al.* (2013); iRVT, inverse random vibration theory.

information is more uncertain. Authors who have included small-magnitude data in GMPE development (e.g., Bommer *et al.*, 2007; Chiou *et al.*, 2010) have concluded that (1) GMPEs should be derived using data at least one magnitude unit below that required for their target application and (2) the aleatory variability significantly increases as a result of including small-magnitude data.

Because the PSHA for the new Swiss national seismic-hazard maps uses a rather low minimum magnitude of 4, we had to ensure that all the selected empirical GMPEs are valid at this magnitude. To this end, we followed the methodology developed during the PEGASOS Refinement project (Stafford, 2011) and subsequently used elsewhere (e.g., Bourne *et al.*, 2015), in which the small magnitude adjusted (SMA) GMPE Y_{SMA} is given by

$$Y_{\mathrm{SMA}} = Y - \delta(M, R|T), \tag{3}$$

in which

$$\delta(M, R|T) = \left(\frac{M_{\mathrm{ref}} - M}{a}\right)^b \left(c + d \ln\left(\frac{\max(\min(R, R_{\max}), R_{\min})}{R_{\mathrm{ref}}}\right)\right), \quad M \le M_{\mathrm{ref}} \tag{4}$$

and

$$\delta(M, R|T) = 0, \quad M > M_{\mathrm{ref}}. \tag{5}$$

Y is the original GMPE prediction (in terms of natural logarithms). M_{ref} is chosen based on the magnitude above which the GMPE is trusted (we set $M_{\mathrm{ref}} = 5.5$). $R_{\mathrm{ref}} = 20$ km is a generic distance chosen as a reference, wheras the coefficients (a to d) are determined through regressions on the residual misfit of a specific GMPE to the locally recorded small-magnitude data. $R_{\min} = 10$ km and $R_{\max}$ (determined through regression) are the minimum and maximum distances used for the correction, respectively. An example of small magnitude adjustment applied to the model AB10 is shown in Figure 4 and the coefficients are shown in Table 3. Ⓔ The adjustments applied to the other empirical models are provided in Tables S5–S12. Recorded Swiss foreland and alpine

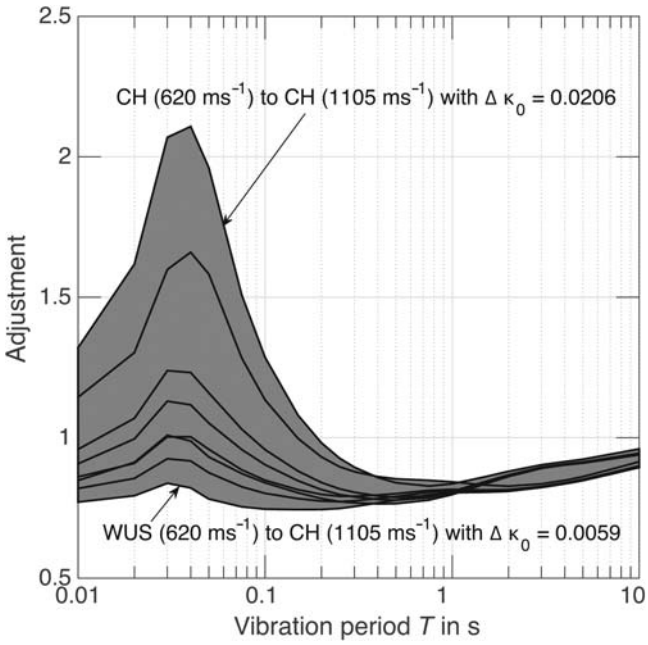

Figure 3. Summary of the V_S−κ_0 adjustments for the CY08 GMPE. WUS, western United States rock profile; CH, Swiss reference-rock profile.

data for events with magnitude ranging between 3.3 and 3.7 are shown as symbols in Figure 4. The original (nonadjusted) GMPE for M_{w} 3.5 clearly overpredicts the median observations. The fully adjusted GMPE (SMA and V_S−κ_0) is shown to reasonably match the data distribution and the Swiss model of Edwards and Fäh (2013b) (hereafter referred to as EF13). It is apparent from Figure 4 that the SMA is much stronger than the V_S−κ_0 adjustment for small magnitude events, to the extent that uncertainties involved in defining the SMA would make any V_S−κ_0 adjustment statistically insignificant. However, it is important to put these corrections into the context of seismic hazard. From hazard disaggregation, we know that tectonic hazard is dominated by moderate-to-large earthquakes (e.g., $\mathbf{M} \sim 6$–7) at short distances (e.g., $R_{\mathrm{JB}} \sim 30$ km). For such events the SMA is zero, while the V_S−κ_0 leads to changes in the rock ($V_{S30} \sim 620$ m/s) motions, in the case of CY08, of up to a factor of 2 at 20 Hz (Fig. 3). Although the SMA is, therefore, clearly more dramatic for the smallest events considered in PSHA, it is the combined effect of both SMA and any V_S−κ_0 adjustment that will affect the final hazard. Because of the limited influence of small magnitude events on ground-motion exceedance (particularly when the predicted motions are reduced by the SMA), it is therefore the V_S−κ_0 adjustment that has the biggest impact on the final hazard estimates.

Figure 5 shows the median PSA($T = 0.2$ s; $\zeta = 5\%$) predictions of the simulation-based and empirical GMPEs adopted in this study as a function of the hypocentral distance and moment magnitude. The different curves shown for the simulation-based stochastic model correspond to different values of the stress parameter $\Delta\sigma$, as explained in the

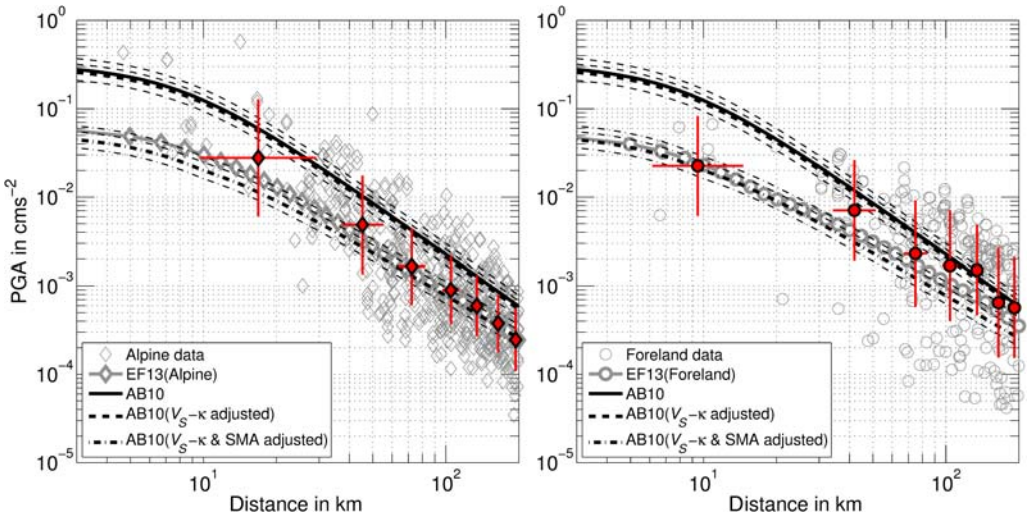

Figure 4. V_S–κ_0 and small magnitude adjustment (SMA) for the Akkar and Bommer (2010; referred as AB10) predictive model for peak ground acceleration (PGA) at M_w 3.5, compared with recorded Swiss small-magnitude data ($3.3 \leq M_w \leq 3.7$) and the stochastic model of Edwards and Fäh (2013b; referred as EF13). For the adjusted models, thin lines indicate the individual adjustments used in the logic tree, thick lines indicate the uniform average. (left panel) Alpine data and EF13 model; (right panel) foreland data and EF13 model. Filled symbols with error bars indicate bin averages and standard deviation. The color version of this figure is available only in the electronic edition.

Adopted Logic Tree section. Note the different amplitude and shape of attenuation with distance of the Swiss stochastic models in the Swiss Alps and foreland (Edwards and Fäh, 2013b; Cauzzi, Edwards, *et al.*, 2015). For each empirical model, three curves corresponding to alternative V_S–κ_0 adjustments are plotted. The straight lines correspond to the model CF08 that does not implement a saturation term, because it is calibrated for hypocentral distances larger than 15 km. As apparent from Figure 5, without considering any weighting, the entire set of empirical and stochastic-median predictions spans roughly one order of magnitude in PSA ($T = 0.2$ s; $\zeta = 5\%$) over a broad distance range. For $M_w \geq 6$, the lower bound of the median predictions is given by the model EF13 for $\Delta\sigma = 1$ MPa (considered valid for shallow [depth < 6 km] crustal events), whereas the upper bound is the model of CF08. At lower magnitudes, the upper bound of the median predictions is the model EF13 for $\Delta\sigma = 12$ MPa. As shown in Figure 5, for the higher values of $\Delta\sigma$ (≥ 5 MPa), the stochastic and empirical models are broadly comparable. Only the lowest three models ($\Delta\sigma \leq 3$ MPa), considered valid for shallow seismicity, show significantly different predictions. Although GMPEs are known to provide robust predictions throughout the magnitude range of interest, none have been developed specifically in Switzerland. Furthermore, they are likely dominated by a deeper focus (and therefore higher stress parameter events) (e.g., Hough, 2014), which our logic tree aims to specifically separate. We therefore feel that, although these models do predict relatively low amplitudes compared with global GMPEs, their inclusion within the logic-tree framework is justified due to their consistency with both small magnitude weak-motion data and large-magnitude macroseismic data in the specific setting of the shallow (depth < 6 km) crust.

Prediction Uncertainties

GMPEs are multi-degree-of-freedom models that require careful fitting to derive robust coefficients and to avoid trade-offs between the source, path, and site effects. Typically, the fitting of the GMPE to the data is done using a multistage maximum-likelihood approach (Joyner and Boore, 1993) or more commonly for recent GMPEs, the random-effects approach (Abrahamson and Youngs, 1992). The misfit of a GMPE to the data used to derive it (represented as the standard deviation of log-space residuals, σ_T) is considered as total uncertainty. Then σ_T is split into at least a between-event (also called interevent) τ and a within-event (or intra-event) uncertainty component φ to isolate event-specific and path-site-specific-aleatory variability (randomness):

$$\sigma_T = \sqrt{\tau^2 + \varphi^2}. \tag{6}$$

This is an important feature used in seismic-hazard analysis to appropriately incorporate the lower variability ground motion expected from a single event (φ), with respect to the average variability over many events (σ_T). Recent work has shown the importance of further decoupling uncertainty in GMPEs and the subsequent (partial) removal of the ergodic assumption (Rodriguez-Marek *et al.*, 2013). The ergodic assumption used to develop GMPEs is that the ground motion observed in the spatial domain (i.e., over numerous recording sites) is reflective of the ground motion observed in the time domain (i.e., at one site). A problem with this approach is that the site-to-site variability is mapped into the within-event uncertainty measure of GMPEs. However, when computing hazard, or simply examining scenario events, we use a reference site (in our case Poggi *et al.*, 2011). Including

Table 3
Coefficients Used for Equation (4) with the Model of Akkar and Bommer (2010)

Period (s)	a	b	c	d	R_{max} (km)	R_{min} (km)	R_{ref} (km)	M_{ref}
0.010	1.415563	1.239239	0.995590	−0.216847	1972.3	10.0	20.0	5.50
0.020	1.258943	1.000000	0.994693	−0.245797	1144.3	10.0	20.0	5.50
0.030	1.278509	1.000000	0.996465	−0.237767	1322.2	10.0	20.0	5.50
0.040	1.277566	1.042382	0.996425	−0.277362	868.9	10.0	20.0	5.50
0.050	1.276418	1.077745	0.996358	−0.309346	501.0	10.0	20.0	5.50
0.100	1.433038	1.222753	0.996372	−0.400643	240.5	10.0	20.0	5.50
0.150	1.384642	1.250938	0.996417	−0.319041	631.1	10.0	20.0	5.50
0.200	1.350304	1.271328	0.996450	−0.261144	908.2	10.0	20.0	5.50
0.250	1.517877	1.262536	0.996806	−0.275018	766.5	10.0	20.0	5.50
0.300	1.654794	1.255398	0.997098	−0.286355	650.7	10.0	20.0	5.50
0.350	1.855761	1.322266	0.996444	−0.328013	467.2	10.0	20.0	5.50
0.400	2.030328	1.383505	0.995872	−0.364282	307.8	10.0	20.0	5.50
1.000	−5.169560	1.000000	1.010650	0.622190	N/A	10.0	20.0	5.50
1.050	−6.821261	1.000000	1.016859	0.833713	N/A	10.0	20.0	5.50
1.100	−8.396109	1.000000	1.022780	1.035395	N/A	10.0	20.0	5.50
1.150	−9.900941	1.000000	1.028437	1.228109	N/A	10.0	20.0	5.50
1.200	−11.341718	1.000000	1.033854	1.412621	N/A	10.0	20.0	5.50
1.250	−12.723671	1.000000	1.039049	1.589599	N/A	10.0	20.0	5.50
1.300	−14.051415	1.000000	1.044041	1.759635	N/A	10.0	20.0	5.50
1.350	−15.329044	1.000000	1.048844	1.923254	N/A	10.0	20.0	5.50
1.400	−16.560203	1.000000	1.053472	2.080921	N/A	10.0	20.0	5.50
1.450	−17.748154	1.000000	1.057938	2.233055	N/A	10.0	20.0	5.50
1.500	−18.895828	1.000000	1.062253	2.380030	N/A	10.0	20.0	5.50
1.550	−20.005867	1.000000	1.066426	2.522186	N/A	10.0	20.0	5.50
1.600	−21.080660	1.000000	1.070467	2.659828	N/A	10.0	20.0	5.50
1.650	−22.122377	1.000000	1.074383	2.793235	N/A	10.0	20.0	5.50
1.700	−23.132994	1.000000	1.078182	2.922658	N/A	10.0	20.0	5.50
1.750	−24.114313	1.000000	1.081872	3.048330	N/A	10.0	20.0	5.50
1.800	−25.067986	1.000000	1.085457	3.170461	N/A	10.0	20.0	5.50
1.850	−25.995527	1.000000	1.088944	3.289246	N/A	10.0	20.0	5.50
1.900	−26.898331	1.000000	1.092338	3.404863	N/A	10.0	20.0	5.50
1.950	−27.777683	1.000000	1.095644	3.517476	N/A	10.0	20.0	5.50
2.000	−28.634770	1.000000	1.098866	3.627238	N/A	10.0	20.0	5.50
2.050	−28.634770	1.000000	1.098866	3.627238	N/A	10.0	20.0	5.50
2.100	−28.634770	1.000000	1.098866	3.627238	N/A	10.0	20.0	5.50
2.150	−28.634770	1.000000	1.098866	3.627238	N/A	10.0	20.0	5.50
2.200	−28.634770	1.000000	1.098866	3.627238	N/A	10.0	20.0	5.50
2.250	−28.634770	1.000000	1.098866	3.627238	N/A	10.0	20.0	5.50
2.300	−28.634770	1.000000	1.098866	3.627238	N/A	10.0	20.0	5.50
2.350	−28.634770	1.000000	1.098866	3.627238	N/A	10.0	20.0	5.50
2.400	−28.634770	1.000000	1.098866	3.627238	N/A	10.0	20.0	5.50
2.450	−28.634770	1.000000	1.098866	3.627238	N/A	10.0	20.0	5.50
2.500	−28.634770	1.000000	1.098866	3.627238	N/A	10.0	20.0	5.50
2.550	−28.634770	1.000000	1.098866	3.627238	N/A	10.0	20.0	5.50
2.600	−28.634770	1.000000	1.098866	3.627238	N/A	10.0	20.0	5.50
2.650	−28.634770	1.000000	1.098866	3.627238	N/A	10.0	20.0	5.50
2.700	−28.634770	1.000000	1.098866	3.627238	N/A	10.0	20.0	5.50
2.750	−28.634770	1.000000	1.098866	3.627238	N/A	10.0	20.0	5.50
2.800	−28.634770	1.000000	1.098866	3.627238	N/A	10.0	20.0	5.50
2.850	−28.634770	1.000000	1.098866	3.627238	N/A	10.0	20.0	5.50
2.900	−28.634770	1.000000	1.098866	3.627238	N/A	10.0	20.0	5.50
2.950	−28.634770	1.000000	1.098866	3.627238	N/A	10.0	20.0	5.50
3.000	−28.634770	1.000000	1.098866	3.627238	N/A	10.0	20.0	5.50
4.000	−28.634770	1.000000	1.098866	3.627238	N/A	10.0	20.0	5.50

R_{max} defined as not applicable (N/A) should be implemented as a sufficiently large value (e.g., 10^{09}) in equation (4).

site-to-site variability in predictions therefore unjustifiably increases the overall prediction uncertainty for this application.

The reality is that in many cases we know the expected site response behavior and its uncertainty. In this case, the so-called single-site sigma (σ_{SS}) can significantly reduce the predicted ground-motion variability and the resultant hazard at long return periods (Atkinson, 2006). Single-site sigma is given by

$$\sigma_{SS} = \sqrt{\tau^2 + \varphi_{SS}^2}, \tag{7}$$

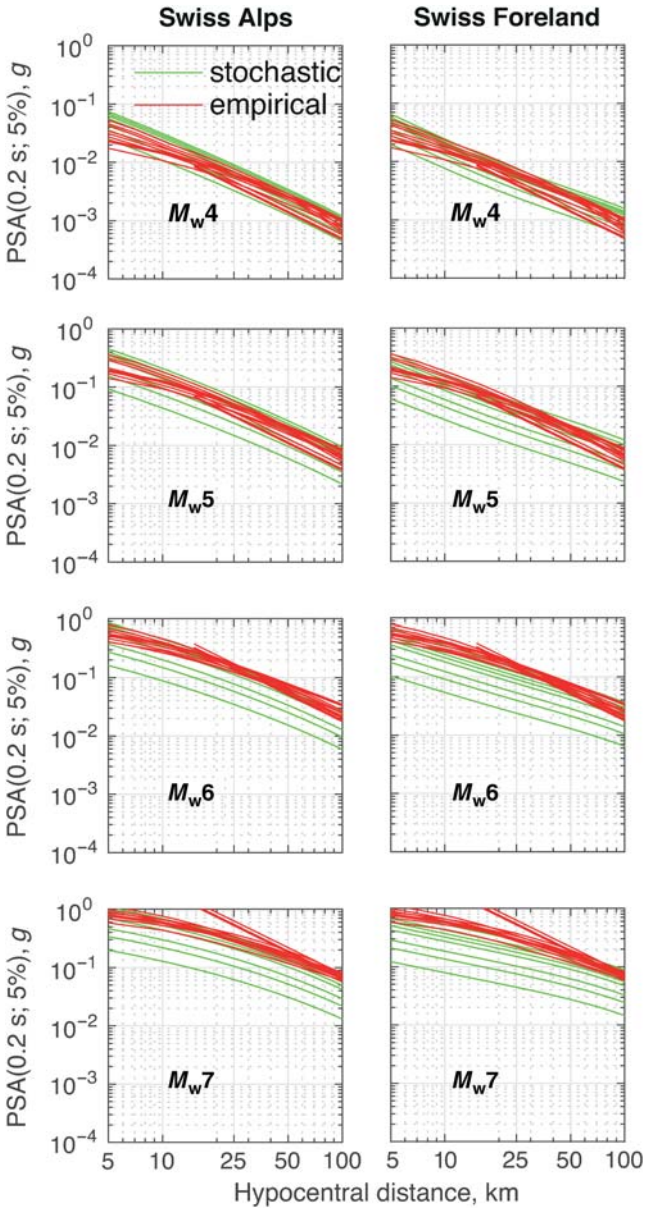

Figure 5. Median predictions of the simulation-based and empirical GMPEs adopted in this study, as a function of the hypocentral distance and moment magnitude. For each empirical model, three curves corresponding to alternative V_S–κ_0 adjustments are plotted in the figure. The color version of this figure is available only in the electronic edition.

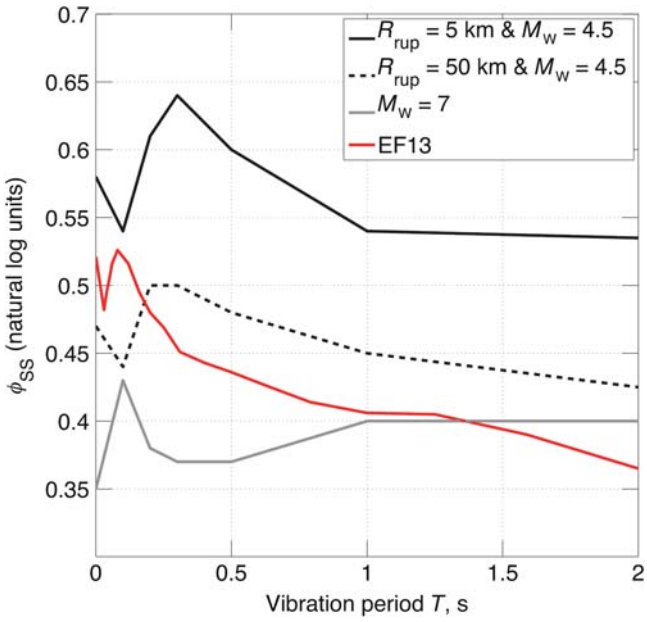

Figure 6. Comparison of the different models of single-station sigma φ_{SS} used in this study. The curves for specific magnitude and distances represent the model of Rodriguez-Marek *et al.* (2013). Note that for $M_w \geq 7$ the model is distance independent. The φ_{SS} model of EF13 is also shown and is a function of vibration period only. The color version of this figure is available only in the electronic edition.

in which φ_{SS} is the within-event uncertainty for a single site, the standard deviation of ground motions observed if we were to record a single earthquake on multiple clones of a given site (at various azimuths, distances, etc.). Rodriguez-Marek *et al.* (2013) determined φ_{SS} for a variety of regions (including Switzerland) and found that it appears, on average, to be regionally independent. They proposed four models to describe φ_{SS}: period dependent, distance-period dependent, magnitude-period dependent, and magnitude-distance-period dependent. Physical reasons for magnitude and distance dependence of ground-motion variability do support a higher variability of ground motion in the near field ($R \lesssim 30$ km), for which complex and highly variable source effects are often observed (e.g., directivity), and for smaller earthquakes which tend to exhibit more variability than larger events (e.g., in terms of source depth, stress drop, etc.).

In this study, we adopted two alternative approaches to model φ_{SS}: (1) the magnitude-, distance-, and period-dependent model by Rodriguez-Marek *et al.* (2013) and (2) the period-dependent average across Switzerland of Edwards and Fäh (2013b), as shown in Figure 6. Note how φ_{SS} decreases with distance for low magnitudes ($M_w \sim 4.5$), whereas it is independent of distance at high magnitudes ($M_w \sim 7$). We defined the total uncertainty using equation (7) with τ taken from the corresponding GMPEs. The variation of σ_T as a function of magnitude and distance for the different empirical and stochastic models used in this study, along with *trellis* plots for all the ground-motion prediction models, is shown in Ⓔ Figures S1–S15.

Adopted Logic Tree

Critical in the Swiss context is the implementation of region-specific ground-motion models (Edwards and Fäh, 2013b) and corresponding predictive equations (Cauzzi, Edwards, *et al.*, 2015). The main reasons are that (a) the attenuation of shear-wave energy is regionally dependent (Edwards *et al.*, 2011); (b) the earthquakes located in the alpine region typically occur at shallower depths than those located in the Swiss foreland (Fäh *et al.*, 2011; Diehl *et al.*, 2013, 2014); and (c) the shallow (depth < 6 km) and deep earthquakes

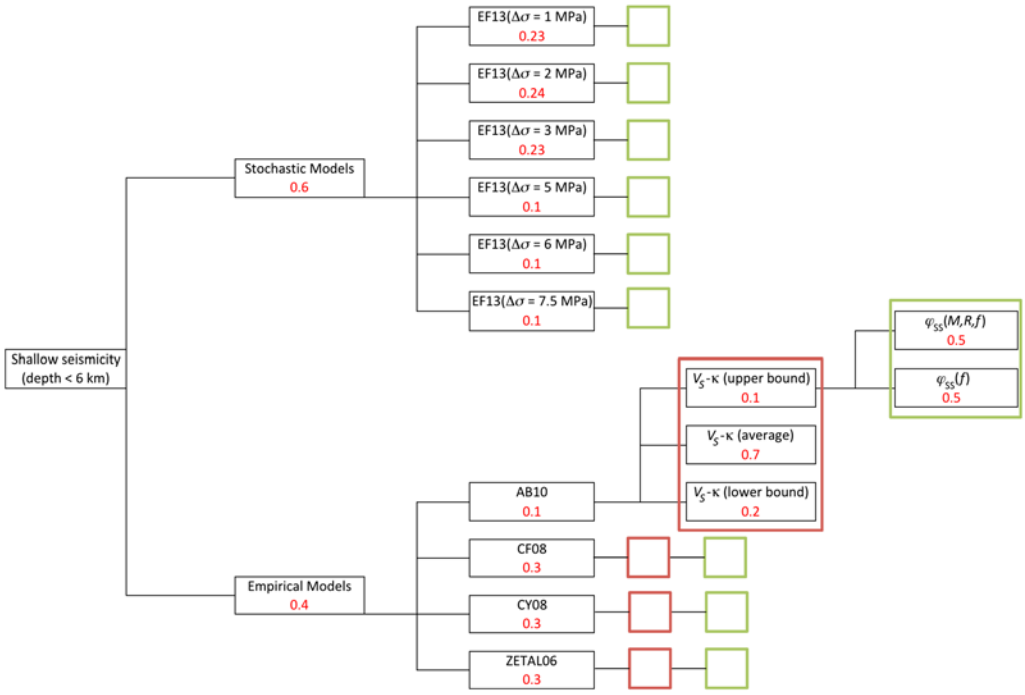

Figure 7. Logic tree for ground-motion prediction models and shallow seismicity (depth < 6 km). CF08, Cauzzi and Faccioli (2008); ZETAL06, Zhao *et al.* (2006). The color version of this figure is available only in the electronic edition.

exhibit different stress parameter values, typically increasing with depth (Goertz-Allmann and Edwards, 2014; Cauzzi, Edwards, *et al.*, 2015).

The logic tree used in this study for shallow seismicity is identical in the Swiss Alps and foreland (Fig. 7), whereas different choices were made for deep seismicity in the two regions (Figs. 8 and 9). Within each seismotectonic context (shallow seismicity, deep alpine seismicity, deep foreland seismicity), the first logic-tree branching level accounts for the availability of stochastic and empirical prediction models, weighted 0.6 and 0.4, respectively. We assigned more weight to the stochastic predictions because they were specifically derived for Switzerland, with separation of shallow and deep, foreland, and alpine seismicity that has been calibrated against macroseismic and instrumental data. However, we do not exceed 60% weight to penalize the synthetic nature of the predictions, which leads to increased epistemic uncertainty at higher magnitudes (e.g., $M_w > 6.5$). Furthermore, we believe that by using the small magnitude and V_S–κ_0 corrections, the empirical models present a suitable means for predicting ground-motion amplitudes in Switzerland. The empirical prediction models are all weighted 0.3 apart from AB10 that contributes 10%. This is due to the relatively simplistic ground-type classification used by AB10 that resulted in comparatively less effective V_S–κ_0 corrections, as shown by a careful scrutiny of the PSA spectral shapes obtained after the adjustment.

For each empirical prediction model, the subsequent branching level accounts for the V_S–κ_0 adjustments. We picked three V_S–κ_0 models representative of the average, minimum, and maximum amplification with respect to the target-rock profile of Poggi *et al.* (2011), with weights equal to 0.7, 0.2, and 0.1, respectively, thus penalizing large amplifications and de-amplifications of the original GMPEs. This is valid for all models apart from CF08 that takes weights 0.4, 0.3, and 0.3, due to comparatively less-scattered results of the V_S–κ_0 adjustments (more gentle variation of spectral shapes).

The weighting scheme adopted for the stochastic models is consistent with the findings of Cauzzi, Edwards, *et al.* (2015) who tested Edwards and Fäh (2013b) with different values of stress parameter $\Delta\sigma$ against a dataset of ~2000 EMS-98 intensity data points available in the earthquake catalog of Switzerland ECOS-09 (Fäh *et al.*, 2011), generated by events with $4.7 < M_w < 6.6$ and distances within 230 km of the earthquake source. Stochastic predictions of shallow events are based on six different values of $\Delta\sigma$ in EF13, namely 1, 2, 3, 5, 6, and 7.5 MPa, with weights 0.23, 0.24, 0.23, 0.1, 0.1, and 0.1, respectively. For deep events we use $\Delta\sigma = 5$, 6, 7.5, and 9 MPa in the Swiss foreland and $\Delta\sigma = 6$, 7, 9, and 12 MPa in the Swiss Alps, with weights equal to 0.35, 0.35, 0.2, and 0.1, respectively.

The last branching level for both empirical and stochastic models accounts for the epistemic uncertainty in modeling single-station sigma, as presented in the Prediction Uncertainties section. Adopting an equal weight means that we consider both models as alternative options. Sensitivity analyses performed on the two alternative models showed a difference of ~5% on the mean ground-shaking estimates.

Figure 10 shows the hazard curves (5, 16, 50, 84, and 95 percentile levels) for the city of Basel located in the Swiss

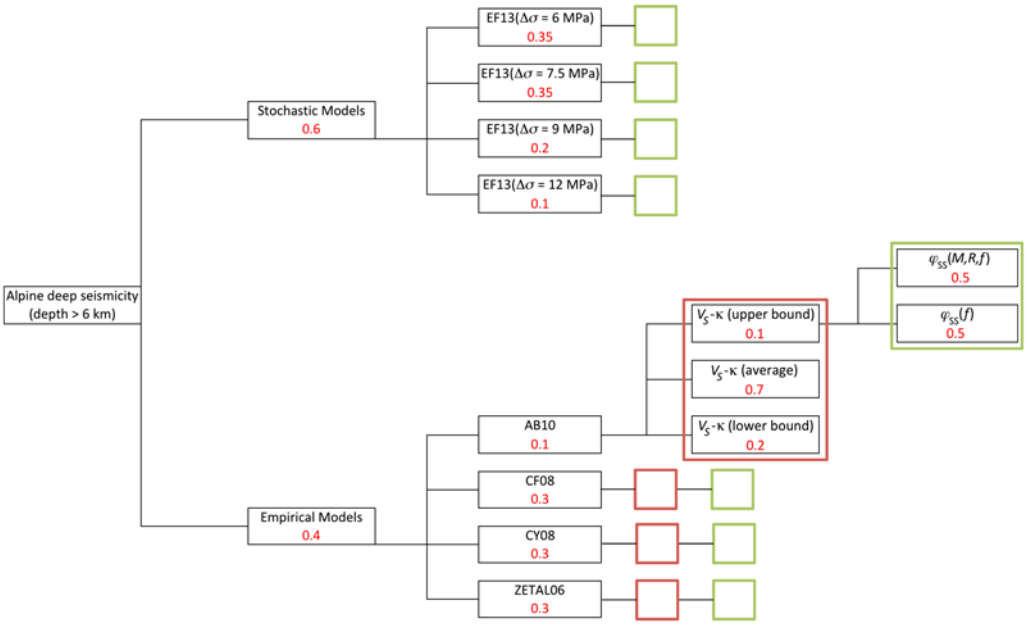

Figure 8. Logic tree for ground-motion prediction models for deep (depth > 6 km) alpine seismicity. The color version of this figure is available only in the electronic edition.

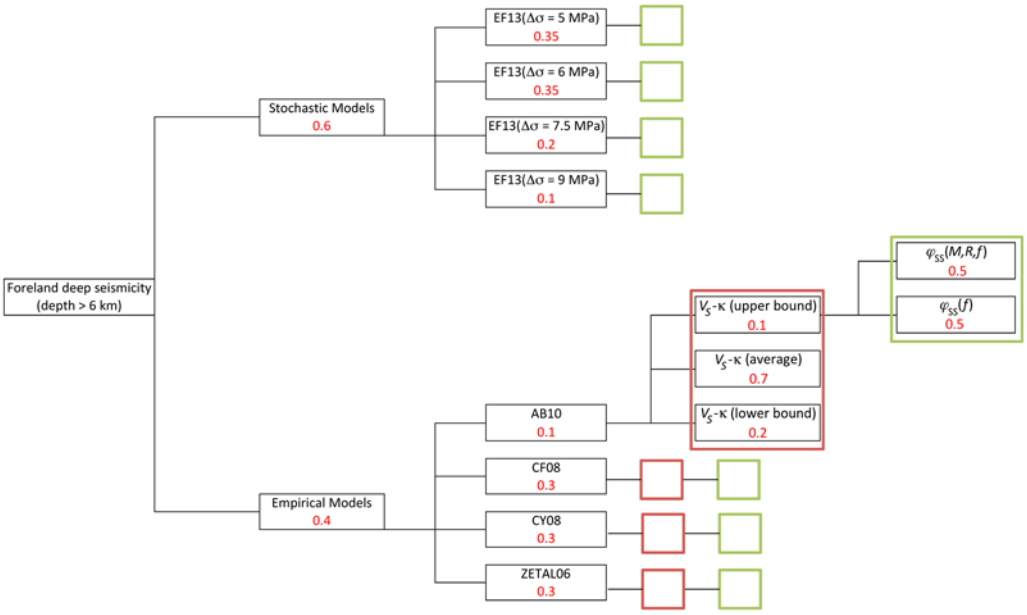

Figure 9. Logic tree for ground-motion prediction models for deep (depth > 6 km) events in the Swiss foreland. The color version of this figure is available only in the electronic edition.

foreland region (the location of the largest historical central European earthquake on record, with M_w 6.6), at the border among Switzerland, Germany, and France. Hazard is expressed as the probability of exceedance of a given spectral acceleration level in 50 years. Note how the empirical models yield significantly higher hazard levels than the stochastic models in the Swiss foreland at all vibration periods, even after host-to-target and small magnitude adjustment. The empirical branches are effectively equivalent to 84th-percentile levels of the total hazard, while the stochastic models (specifically calibrated for Switzerland) tend to lie within the median and the 16th percentile of the total hazard.

In the Swiss Alps (Fig. 11), the average hazard levels yielded by the stochastic model tend to match the median values of the total hazard at all vibration periods for acceleration levels lower than 2g. The empirical branches contribute with generally slightly higher hazard values, although they never reach or exceed the 84th percentile of the total hazard at short

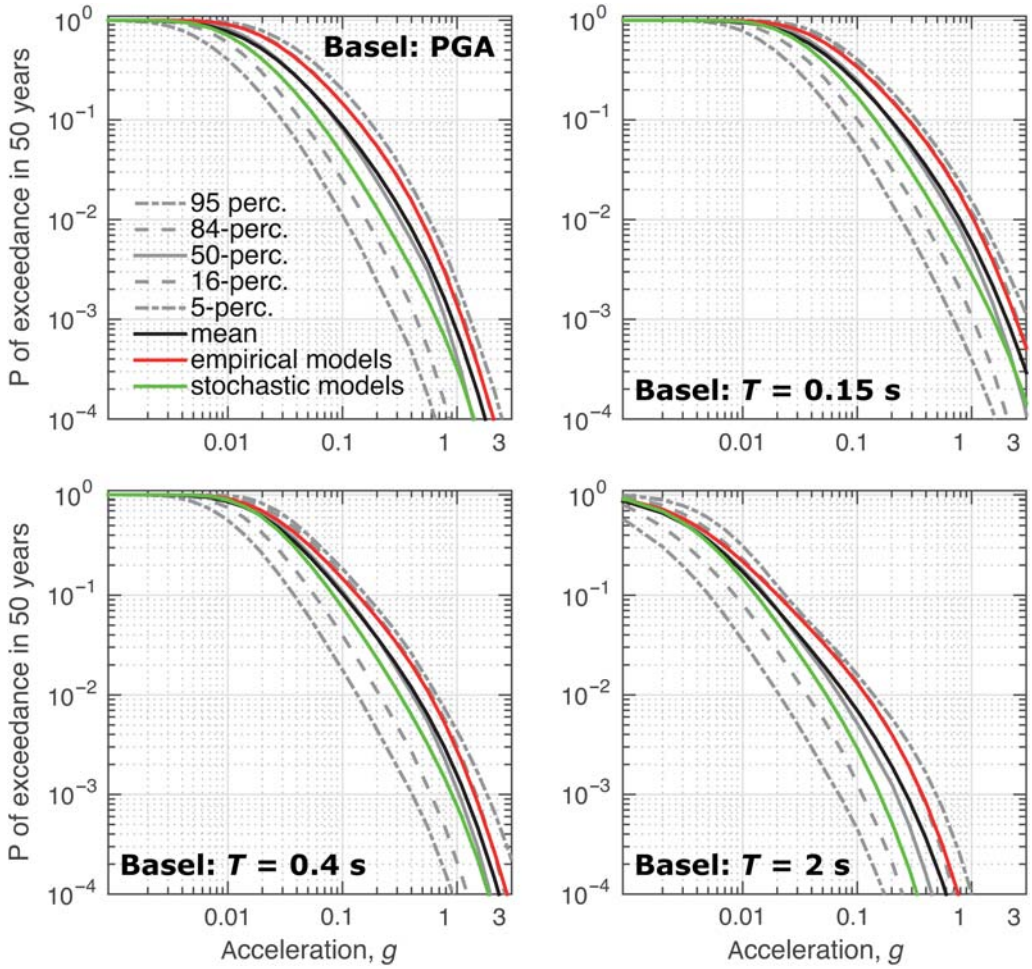

Figure 10. Hazard curves for the city of Basel located in the Swiss foreland region. Total hazard estimates (mean and percentiles) are indicated along with hazard levels obtained considering the empirical or stochastic prediction models only. The color version of this figure is available only in the electronic edition.

periods. Significant differences are apparent at $T = 2$ s, for which the average hazard produced by the empirical models matches the 84th percentile of the total hazard.

Figure 12 shows uniform hazard spectra for Sion and Basel and two different return periods, namely $T_R = 475$ years (used for design and assessment of residential buildings) and 10,000 years (used for design and assessment of special structures and infrastructure, such as dams). As anticipated from Figures 9 and 10, the empirical predictions tend to systematically exceed the stochastic predictions over a broad period range both in the Alps and the foreland, the only exception being the case of Sion at $T_R = 10{,}000$ years and $T \sim 0.05$ s. In Sion, the mean predictions yielded by the stochastic models are in good agreement with the mean total hazard. In Basel, the empirical predictions typically match the 84th percentile of the total hazard for $T > 0.1$ s. Although the peak of the uniform hazard spectrum (UHS) is at 0.1 s for both the stochastic and empirical models (and therefore the total hazard as well), the latter tend to show a different spectral shape with comparatively more energy at 0.15 and 0.2 s. This reflects part of the epistemic uncertainties of the ground-motion models. We note, however, that the spectral shapes of the empirical models might result as well from poorly constrained host-rock conditions, as discussed in the previous sections. The total hazard UHS computed for Sion and Basel would support using $T_B = 0.05$ s as the lower bound of the constant acceleration branch of the design spectrum. Finally, we note that the full 2015 Swiss national seismic hazard model has been implemented within the online European Facility for Earthquake Hazard and Risk, which can be used to easily obtain user-defined hazard maps, exceedance curves, and UHS at any point in Switzerland.

Conclusions

We presented the assessment, adjustment, and weighting of ground-motion prediction models adopted for the current update of the Swiss national seismic-hazard maps delivered by the Swiss Seismological Service. The hazard estimates are based on bringing together the best elements of both empirical and stochastic ground-motion prediction models. We used only consolidated empirical models largely used and

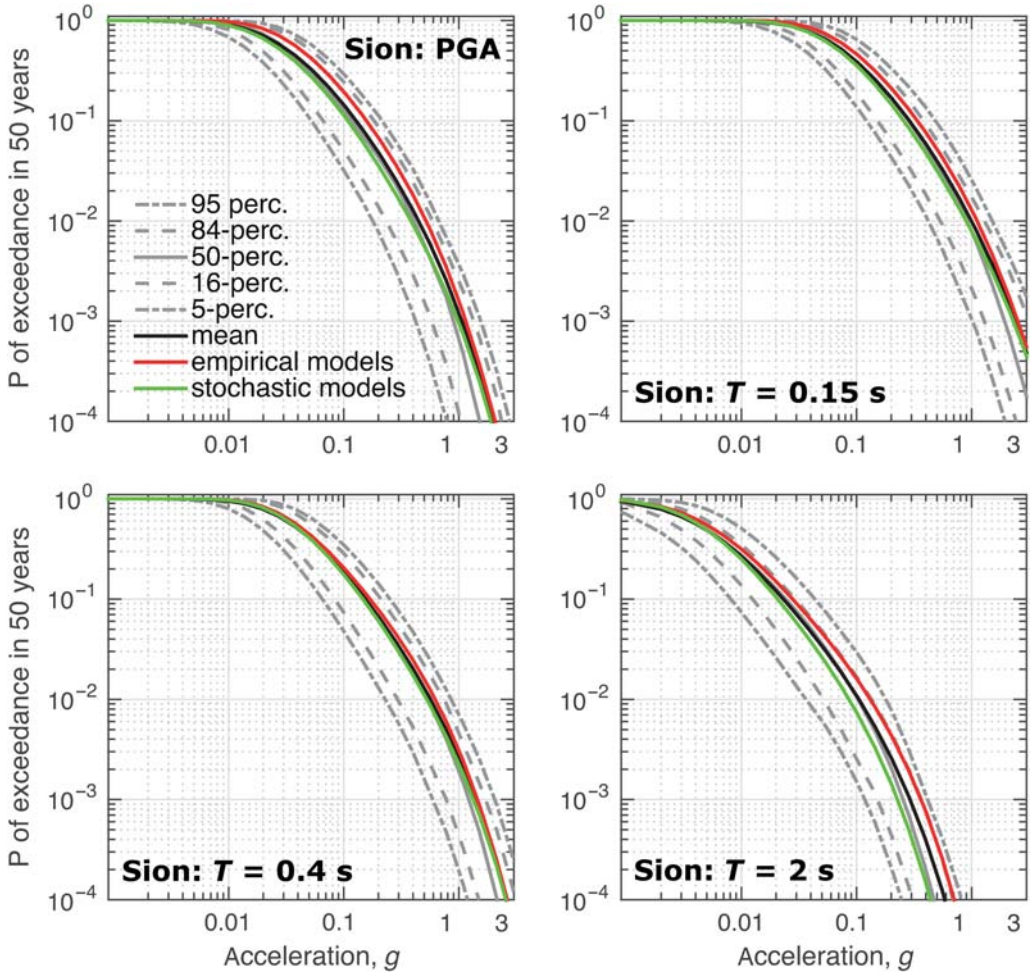

Figure 11. As Figure 10 but for the town of Sion, in the Swiss Alps. The color version of this figure is available only in the electronic edition.

tested in Europe and worldwide, namely those of ZETAL06, CY08, CF08, and AB10. Although we are aware that the release of an updated GMPE by the same authors generally supersedes previous models and should therefore be preferred, users' experience shows that potential issues with newly published GMPEs are generally spotted several months after the release through testing in several applied research projects. We decided not to take this risk in the update of the national Swiss seismic hazard maps and to rely on consolidated models, in which strengths and deficiencies we believe are well informed. As to the stochastic models, we adopted the Swiss-specific prediction of EF13 that is based on a well-defined Swiss reference-rock profile by Poggi *et al.* (2011). This marks a significant discontinuity with respect to traditional empirical ground-motion prediction studies, for which the definition of the reference rock through ground types determined by the surface geology and V_{S30} values (often estimated and not measured) can be vague and incomplete. Consistent with the most recent state-of-the-art in ground-motion characterization for PSHA (Coppersmith *et al.*, 2014; Renault, 2014), we adjusted the empirical predictive models to match the amplification and attenuation levels typical of the Swiss reference rock and made them suitable for predictions at moderate-to-low magnitudes (Stafford, 2011) typical of the instrumentally recorded seismicity of the greater Swiss region. The uncertainty estimates in our updated hazard model are based on single-station sigma values obtained through two alternative approaches: using a regionally independent model for within-event ground-motion variability (Rodriguez-Marek *et al.*, 2013) and using Swiss-specific within-event ground-motion variability (Edwards and Fäh, 2013b).

The update of the Swiss national seismic hazard has taken advantage of significant recent advances in ground-motion characterization. The resulting median predictions (and epistemic uncertainty) consequently represent a step change in quality compared with previous models and reflects state-of-the-art practice typically reserved for PSHA at nuclear power stations. The move toward nonergodic (single-station) sigma leads to a reduction in exceedance levels (and hence seismic hazard) at long return periods. The choices documented in the present study provide a methodological framework for region-specific ground-motion characterization within PSHA. While applied to the development of the Swiss national seismic hazard maps, the scope of this article is significantly beyond this

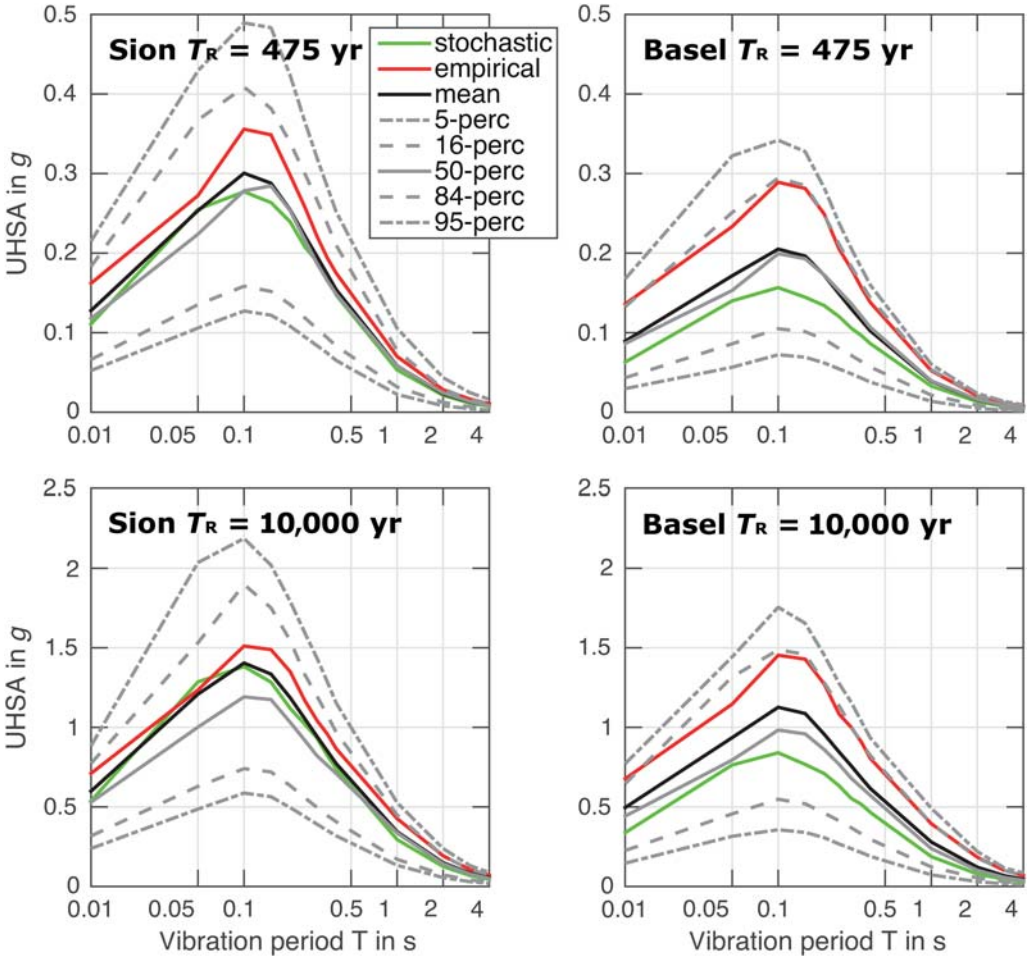

Figure 12. Uniform hazard spectral acceleration (UHSA) as a function of vibration period T for Sion (Swiss Alps, left panels) and Basel (Swiss foreland, right panels) and two different return periods, namely (top panels) 475 years and (bottom panels) 10,000 years. The mean and percentiles of the total hazard are indicated along with the mean acceleration levels obtained using the stochastic or empirical branches only. The color version of this figure is available only in the electronic edition.

application, with usage particularly suited to regions of low-to-moderate seismicity.

Data and Resources

A summary of the Swiss National Seismic Hazard Maps 2015 can be viewed online at http://www.seismo.ethz.ch/eq_swiss/Erdbebengefaehrdung/index_EN (last accessed March 2016), whereas the European Facility for Earthquake Hazard and Risk (EFHAR) can be used for interactive viewing of the hazard map, exceedance curves, and uniform hazard spectra at www.efehr.org (last accessed March 2016). Douglas (2015) provides a summary of the empirical GMPEs used in this study, and can be downloaded from http://www.gmpe.org.uk (last accessed December 2015). The Swiss specific adjusted GMPEs are available under open-source license at https://github.com/gem/oq-hazardlib/tree/master/openquake/hazardlib/gsim (last accessed March 2016). The computer program Strata (Kottke and Rathje, 2008) can be downloaded from https://nees.org/resources/strata (last accessed December 2015).

Acknowledgments

We are indebted to our colleagues Stefan Wiemer, Domenico Giardini, Florian Haslinger, Philipp Kaestli, Edi Kissling, Jochen Woessner (now at Risk Management Solutions), Valerio Poggi (now at the Global Earthquake Model Foundation), Clotaire Michel, Stefan Hiemer, and numerous others at the Swiss Seismological Service with whom we have worked on the updated Swiss Seismic Hazard Maps. We thank Associate Editor Mark Stirling and two anonymous reviewers who provided useful comments on this article.

References

Abrahamson, N., and W. Silva (2008). Summary of the Abrahamson & Silva NGA ground-motion relations, *Earthq. Spectra* **24,** 67–97.

Abrahamson, N., P. Birkhauser, M. Koller, D. Mayer-Rosa, P. Smit, C. Sprecher, S. Tinic, and R. Graf (2002). PEGASOS—A comprehensive probabilistic seismic hazard assessment for nuclear power plants in Switzerland, *Proc. of the Twelfth European Conference on Earthquake Engineering*, London, United Kingdom, 9–13 September 2002.

Abrahamson, N. A., and R. R. Youngs (1992). A stable algorithm for regression analyses using the random effects model, *Bull. Seismol. Soc. Am.* **82,** 505–510.

Akkar, S., and J. J. Bommer (2010). Empirical equations for the prediction of PGA, PGV, and spectral accelerations in Europe, the Mediterranean Region, and the Middle East, *Seismol. Res. Lett.* **81,** 195–206.

Akkar, S., and Z. Cagnan (2010). A local ground-motion predictive model for Turkey, and its comparison with other regional and global ground-motion models, *Bull. Seismol. Soc. Am.* **100,** 2978–2995.

Akkar, S., M. A. Sandikkaya, M. Senyurt, A. A. Sisi, B. O. Ay, P. Traversa, J. Douglas, F. Cotton, L. Luzi, B. Hernandez, and S. Godey (2014). Reference database for seismic ground-motion in Europe (RESORCE), *Bull. Earthq. Eng.* **12,** 311–339.

Al Atik, L., A. Kottke, N. Abrahamson, and J. Hollenback (2014). Kappa (κ) scaling of ground-motion prediction equations using an inverse random vibration theory approach, *Bull. Seismol. Soc. Am.* **104,** 336–346.

Ambraseys, N., P. Smit, J. Douglas, B. Margaris, R. Sigbjörnsson, S. Olafsson, P. Suhadolc, and G. Costa (2004). Internet site for European strong-motion data, *Bull. Geof. Teor. Appl.* **45,** 113–129.

Ancheta, T. D., R. B. Darragh, J. P. Stewart, E. Seyhan, W. J. Silva, B. S. Chiou, K. E. Wooddell, R. W. Graves, A. R. Kottke, and D. M. Boore (2014). NGA-West2 database, *Earthq. Spectra* **30,** no. 3, 989–1005, doi: 10.1193/070913EQS197M.

Anderson, J. G., and S. E. Hough (1984). A model for the shape of the Fourier amplitude spectrum of acceleration at high-frequencies, *Bull. Seismol. Soc. Am.* **74,** 1969–1993.

Atkinson, G. M. (2006). Single-station sigma, *Bull. Seismol. Soc. Am.* **96,** 446–455.

Atkinson, G. M., and D. M. Boore (2006). Earthquake ground-motion prediction equations for eastern North America, *Bull. Seismol. Soc. Am.* **96,** 2181–2205.

Atkinson, G. M., and W. Silva (2000). Stochastic modeling of California ground motions, *Bull. Seismol. Soc. Am.* **90,** 255–274.

Bay, F., D. Fäh, L. Malagnini, and D. Giardini (2003). Spectral shear-wave ground-motion scaling in Switzerland, *Bull. Seismol. Soc. Am.* **93,** 414–429.

Bay, F., S. Wiemer, D. Fäh, and D. Giardini (2005). Predictive ground motion scaling in Switzerland: Best estimates and uncertainties, *J. Seismol.* **9,** 223–240.

Bindi, D., F. Pacor, L. Luzi, R. Puglia, M. Massa, G. Ameri, and R. Paolucci (2011). Ground motion prediction equations derived from the Italian strong motion database, *Bull. Earthq. Eng.* **9,** 1899–1920.

Bommer, J. J., B. Dost, B. Edwards, P. J. Stafford, J. v. Elk, D. Doornhof, and M. Ntinalexis (2016). Developing an application-specific ground-motion model for induced seismicity, *Bull. Seismol. Soc. Am.* **106,** no. 1, 158–173, doi: 10.1785/0120150184.

Bommer, J. J., J. Douglas, F. Scherbaum, F. Cotton, H. Bungum, and D. Fäh (2010). On the selection of ground-motion prediction equations for seismic hazard analysis, *Seismol. Res. Lett.* **81,** 783–793.

Bommer, J. J., P. J. Stafford, J. E. Alarcon, and S. Akkar (2007). The influence of magnitude range on empirical ground-motion prediction, *Bull. Seismol. Soc. Am.* **97,** 2152–2170.

Boore, D. M. (2003). Simulation of ground motion using the stochastic method, *Pure Appl. Geophys.* **160,** 635–676.

Boore, D. M. (2009). Comparing stochastic point-source and finite-source ground-motion simulations: SMSIM and EXSIM, *Bull. Seismol. Soc. Am.* **99,** 3202–3216.

Boore, D. M., and G. M. Atkinson (2008). Ground-motion prediction equations for the average horizontal component of PGA, PGV, and 5%-damped PSA at spectral periods between 0.01 s and 10.0 s, *Earthq. Spectra* **24,** 99–138.

Boore, D. M., and W. B. Joyner (1997). Site amplifications for generic rock sites, *Bull. Seismol. Soc. Am.* **87,** 327–341.

Bourne, S., S. Oates, J. Bommer, B. Dost, J. van Elk, and D. Doornhof (2015). A Monte Carlo method for probabilistic hazard assessment of induced seismicity due to conventional natural gas production, *Bull. Seismol. Soc. Am.* **105,** no. 3, 1721–1738, doi: 10.1785/0120140302.

Campbell, K. W. (2003). Prediction of strong ground motion using the hybrid empirical method and its use in the development of ground-motion (attenuation) relations in eastern North America, *Bull. Seismol. Soc. Am.* **93,** 1012–1033.

Campbell, K. W., and Y. Bozorgnia (2008). NGA ground motion model for the geometric mean horizontal component of PGA, PGV, PGD and 5% damped linear elastic response spectra for periods ranging from 0.01 to 10 s, *Earthq. Spectra* **24,** 139–171.

Cartwright, D. E., and M. S. Longuet-Higgins (1956). The statistical distribution of the maxima of a random function, *Proc. Math. Phys. Sci.* **237,** 212–232.

Cauzzi, C., and J. Clinton (2013). A high- and low-noise model for high-quality strong-motion accelerometer stations, *Earthq. Spectra* **29,** 85–102.

Cauzzi, C., and E. Faccioli (2008). Broadband (0.05 to 20 s) prediction of displacement response spectra based on worldwide digital records, *J. Seismol.* **12,** 453–475.

Cauzzi, C., B. Edwards, D. Fäh, J. Clinton, S. Wiemer, P. Kästli, G. Cua, and D. Giardini (2015). New predictive equations and site amplification estimates for the next-generation Swiss ShakeMaps, *Geophys. J. Int.* **200,** 421–438.

Cauzzi, C., E. Faccioli, M. Vanini, and A. Bianchini (2015). Updated predictive equations for broadband (0.01–10 s) horizontal response spectra and peak ground motions, based on a global dataset of digital acceleration records, *Bull. Earthq. Eng.* **13,** 1587–1612.

Chandler, A. M., N. T. K. Lam, and H. H. Tsang (2006). Near-surface attenuation modelling based on rock shear-wave velocity profile, *Soil Dynam. Earthq. Eng.* **26,** 1004–1014.

Chiou, B., R. Darragh, N. Gregor, and W. Silva (2008). NGA project strong-motion database, *Earthq. Spectra* **24,** 23–44.

Chiou, B., R. Youngs, N. Abrahamson, and K. Addo (2010). Ground-motion attenuation model for small-to-moderate shallow crustal earthquakes in California and its implications on regionalization of ground-motion prediction models, *Earthq. Spectra* **26,** 907–926.

Chiou, B. S. J., and R. R. Youngs (2008). An NGA model for the average horizontal component of peak ground motion and response spectra, *Earthq. Spectra* **24,** 173–215.

Clinton, J., C. Cauzzi, D. Fäh, C. Michel, P. Zweifel, M. Olivieri, G. Cua, F. Haslinger, and D. Giardini (2011). The current state of strong motion monitoring in Switzerland, in *Earthquake Data in Engineering Seismology: Predictive Models, Data Management and Networks*, S. Akkar, P. Gülkan, and T. v. Eck (Editors), Springer, Dordrecht, The Netherlands.

Coppersmith, K., J. Bommer, K. Hanson, J. Unruh, R. Coppersmith, L. Wolf, R. Youngs, A. Rodriguez-Marek, L. Al Atik, and G. Toro (2014). Hanford sitewide probabilistic seismic hazard analysis, *PNNL-23361*, Pacific Northwest National Laboratory, Richland, Washington, http://www.hanford.gov/page.cfm/OfficialDocuments/HSPSHA (last accessed May 2016).

Cornell, C. A. (1968). Engineering seismic risk analysis, *Bull. Seismol. Soc. Am.* **58,** 1583–1606.

Cua, G., and T. Heaton (2008). New Ground Motion Prediction Equations Spanning Weak and Strong Motion Levels, *AGU Fall Meeting Abstracts* Abstract S51A-0230.

Dalguer, L. A., H. Miyake, S. M. Day, and K. Irikura (2008). Surface rupturing and buried dynamic-rupture models calibrated with statistical observations of past earthquakes, *Bull. Seismol. Soc. Am.* **98,** 1147–1161.

Delavaud, E., F. Cotton, S. Akkar, F. Scherbaum, L. Danciu, C. Beauval, S. Drouet, J. Douglas, R. Basili, M. A. Sandikkaya, *et al.* (2012). Toward a ground-motion logic tree for probabilistic seismic hazard assessment in Europe, *J. Seismol.* **16,** 451–473.

Diehl, T., J. Clinton, T. Kraft, S. Husen, K. Plenkers, A. Guilhelm, Y. Behr, C. Cauzzi, P. Kastli, F. Haslinger, *et al.* (2014). Earthquakes in Switzerland and surrounding regions during 2013, *Swiss J. Geosci.* **107,** 359–375.

Diehl, T., N. Deichmann, J. Clinton, S. Husen, T. Kraft, K. Plenkers, B. Edwards, C. Cauzzi, C. Michel, P. Kastli, *et al.* (2013). Earthquakes in Switzerland and surrounding regions during 2012, *Swiss J. Geosci.* **106,** 543–558.

Douglas, J. (2015). Ground motion prediction equations 1964–2016, 552 pp., available online at www.gmpe.org.uk (last accessed May 2016).

Douglas, J., S. Akkar, G. Ameri, P. Y. Bard, D. Bindi, J. J. Bommer, S. S. Bora, F. Cotton, B. Derras, M. Hermkes, *et al.* (2014). Comparisons among the five ground-motion models developed using resource for the prediction of response spectral accelerations due to earthquakes in Europe and the Middle East, *Bull. Earthq. Eng.* **12,** 341–358.

Douglas, J., B. Edwards, V. Convertito, N. Sharma, A. Tramelli, D. Kraaijpoel, B. M. Cabrera, N. Maercklin, and C. Troise (2013). Predicting ground motion from induced earthquakes in geothermal areas, *Bull. Seismol. Soc. Am.* **103,** 1875–1897.

Edwards, B., and J. Douglas (2013). Selecting ground-motion models developed for induced seismicity in geothermal areas, *Geophys. J. Int.* **195,** 1314–1322.

Edwards, B., and D. Fäh (2013a). Measurements of stress parameter and site attenuation from recordings of moderate to large earthquakes in Europe and the Middle East, *Geophys. J. Int.* **194,** 1190–1202.

Edwards, B., and D. Fäh (2013b). A stochastic ground-motion model for Switzerland, *Bull. Seismol. Soc. Am.* **103,** 78–98.

Edwards, B., D. Fäh, and D. Giardini (2011). Attenuation of seismic shear wave energy in Switzerland, *Geophys. J. Int.* **185,** 967–984.

Edwards, B., O.-J. Ktenidou, F. Cotton, N. Abrahamson, C. V. Houtte, and D. Fäh (2015). Epistemic uncertainty and limitations of the Kappa0 model for near-surface attenuation at hard rock sites, *Geophys. J. Int.* **202,** no. 3, 1627–1645, doi: 10.1093/gji/ggv222.

Fäh, D., D. Giardini, P. Kästli, N. Deichmann, M. Gisler, G. Schwarz-Zanetti, S. Alvarez-Rubio, S. Sellami, B. Edwards, and B. Allmann (2011). ECOS-09 Earthquake Catalogue of Switzerland Release 2011 Report and Database, Public Catalogue, 17.4.2011. Swiss Seismological Service Eth Zurich, 42 pp., available online at hitseddb.ethz.ch (last accessed May 2016).

Fäh, D., M. Gisler, B. Jaggi, P. Kastli, T. Lutz, V. Masciadri, C. Matt, D. Mayer-Rosa, D. Rippmann, G. Schwarz-Zanetti, *et al.* (2009). The 1356 Basel earthquake: An interdisciplinary revision, *Geophys. J. Int.* **178,** 351–374.

Fritsche, S., and D. Fäh (2009). The 1946 magnitude 6.1 earthquake in the Valais: Site-effects as contributor to the damage, *Swiss J. Geosci.* **102,** 423–439.

Fritsche, S., D. Fäh, M. Gisler, and D. Giardini (2006). Reconstructing the damage field of the 1855 earthquake in Switzerland: Historical investigations on a well-documented event, *Geophys. J. Int.* **166,** 719–731.

Fritsche, S., D. Fäh, and G. Schwarz-Zanetti (2012). Historical intensity VIII earthquakes along the Rhone Valley (Valais, Switzerland): Primary and secondary effects, *Swiss J. Geosci.* **105,** 1–18.

Fritsche, S., D. Fäh, B. Steiner, and D. Giardini (2009). Damage field and site effects: Multidisciplinary studies of the 1964 earthquake series in central Switzerland, *Nat. Hazards* **48,** 203–227.

Giardini, D., D. Giardini, D. Giardini, and S. Erdbebendienst (2004). *Seismic Hazard Assessment of Switzerland, 2004*, Swiss Seismological Service, Swiss Federal Institute (ETH) Zürich, Switzerland.

Giardini, D., J. Wössner, and L. Danciu (2014). Mapping Europe's seismic hazard, *Eos Trans. AGU* **95,** 261–262.

Gisler, M., D. Fäh, and N. Deichmann (2004). The Valais earthquake of December 9, 1755, *Eclogae Geol. Helv.* **97,** 411–422.

Gisler, M., D. Fäh, and P. Kastli (2004). Historical seismicity in central Switzerland, *Eclogae Geol. Helv.* **97,** 221–236.

Gisler, M., D. Fäh, and V. Masciadri (2007). "Terrae Motus Factus Est": Earthquakes in Switzerland before A.D. 1000. A critical approach, *Nat. Hazards* **43,** 63–79.

Gisler, M., D. Fäh, and R. Schibler (2003). Two significant earthquakes in the Rhine Valley at the end of the 18(Th) century: The events of December 6, 1795 and April 20, 1796, *Eclogae Geol. Helv.* **96,** 357–366.

Gisler, M., D. Fäh, and R. Schibler (2004). Revising macroseismic data in Switzerland: The December 20, 1720 earthquake in the region of Lake Constance, *J. Seismol.* **8,** 179–192.

Goertz-Allmann, B. P., and B. Edwards (2014). Constraints on crustal attenuation and three-dimensional spatial distribution of stress drop in Switzerland, *Geophys. J. Int.* **196,** 493–509.

Graves, R. W., and A. Pitarka (2010). Broadband ground-motion simulation using a hybrid approach, *Bull. Seismol. Soc. Am.* **100,** 2095–2123.

Gregor, N., *et al.* (2014). Comparison of NGA-West2 GMPES, *Earthq. Spectra* **30,** 1179–1197.

Hanks, T. C., and R. K. Mcguire (1981). The character of high-frequency strong ground motion, *Bull. Seismol. Soc. Am.* **71,** 2071–2095.

Hiemer, S., J. Woessner, R. Basili, L. Danciu, D. Giardini, and S. Wiemer (2014). A smoothed stochastic earthquake rate model considering seismicity and fault moment release for Europe, *Geophys. J. Int.* **198,** 1157–1170.

Hough, S. E. (2014). Shaking from injection-induced earthquakes in the central and eastern United States, *Bull. Seismol. Soc. Am.* **104,** no. 5, 2619–2626, doi: 10.1785/0120140099.

Johnston, A. C., K. Coppersmith, L. Kanter, and C. Cornell (1994). The earthquakes of stable continental regions. Assessment of large earthquake potential. *EPRI Rept. Tr-102261-V1, 2-1-98*, Palo Alto, California.

Joyner, W. B., and D. M. Boore (1993). Methods for regression-analysis of strong-motion data, *Bull. Seismol. Soc. Am.* **83,** 469–487.

Knopoff, L. (1964). A matrix method for elastic wave problems, *Bull. Seismol. Soc. Am.* **54,** 431–438.

Kottke, A. R., and E. M. Rathje (2008). *Technical Manual for Strata*, University of California, Berkeley, California.

Michel, C., B. Edwards, V. Poggi, J. Burjanek, D. Roten, C. Cauzzi, and D. Fäh (2014). Assessment of site effects in alpine regions through systematic site characterization of seismic stations, *Bull. Seismol. Soc. Am.* **104,** no. 6, 2809–2826, doi: 10.1785/0120140097.

Motazedian, D., and G. M. Atkinson (2005). Stochastic finite-fault modeling based on a dynamic corner frequency, *Bull. Seismol. Soc. Am.* **95,** 995–1010.

Poggi, V., B. Edwards, and D. Fäh (2011). Derivation of a reference shear-wave velocity model from empirical site amplification, *Bull. Seismol. Soc. Am.* **101,** 258–274.

Poggi, V., B. Edwards, and D. Fäh (2013). Reference S-wave velocity profile and attenuation models for ground-motion prediction equations: Application to Japan, *Bull. Seismol. Soc. Am.* **103,** 2645–2656.

Power, M., B. Chiou, N. Abrahamson, Y. Bozorgnia, T. Shantz, and C. Roblee (2008). An overview of the NGA project, *Earthq. Spectra* **24,** 3–21.

Rathje, E., A. Kottke, and C. Ozbey (2005). Using inverse random vibration theory to develop input Fourier amplitude spectra for use in site response, *16th International Conference on Soil Mechanics and Geotechnical Engineering: TC4 Earthquake Geotechnical Engineering Satellite Conference*, 160–166.

Renault, P. (2014). Approach and challenges for the seismic hazard assessment of nuclear power plants: The Swiss experience, *Bull. Geof. Teor. Appl.* **55,** 149–164.

Rietbrock, A., F. Strasser, and B. Edwards (2013). A stochastic earthquake ground-motion prediction model for the United Kingdom, *Bull. Seismol. Soc. Am.* **103,** 57–77.

Rodriguez-Marek, A., F. Cotton, N. A. Abrahamson, S. Akkar, L. Al Atik, B. Edwards, G. A. Montalva, and H. M. Dawood (2013). A model for single-station standard deviation using data from various tectonic regions, *Bull. Seismol. Soc. Am.* **103,** 3149–3163.

Scherbaum, F., F. Cotton, and H. Staedtke (2006). The estimation of minimum-misfit stochastic models from empirical ground-motion prediction equations, *Bull. Seismol. Soc. Am.* **96,** 427–445.

Schwarz-Zanetti, G., N. Deichmann, D. Fäh, D. Giardini, M. J. Jimenez, V. Masciadri, R. Schibler, and M. Schnellman (2003). The earthquake in Unterwalden on September 18, 1601: A historico-critical macroseismic evaluation, *Eclogae Geol. Helv.* **96,** 441–450.

Schwarz-Zanetti, G., N. Deichmann, D. Fäh, V. Masciadri, and J. Goll (2004). The earthquake in Churwalden (Ch) of September 3, 1295, *Eclogae Geol. Helv.* **97,** 255–264.

Silva, V., H. Crowley, M. Pagani, D. Monelli, and R. Pinho (2014). Development of the OpenQuake engine, the global earthquake model's

open-source software for seismic risk assessment, *Nat. Hazards* **72,** 1409–1427.

Silva, W., R. Darragh, N. Gregor, G. Martin, N. Abrahamson, and C. Kircher (1998). Reassessment of site coefficients and near-fault factors for building code provisions, *Technical Report Program Element Ii: 98-Hqgr-1010 Pacific Engineering and Analysis*, El Cerrito, California.

Stafford, P. (2011). *Procedure for Small-Magnitude Extension of GMPES*, Imperial College, London, United Kingdom, 25 pp.

Stafford, P. J. (2014). Crossed and nested mixed-effects approaches for enhanced model development and removal of the ergodic assumption in empirical ground-motion models, *Bull. Seismol. Soc. Am.* **104,** 702–719.

Toro, G. R., N. A. Abrahamson, and J. F. Schneider (1997). Model of strong ground motions from earthquakes in central and eastern North America: Best estimates and uncertainties, *Seismol. Res. Lett.* **68,** 41–57.

Wiemer, S., D. Giardini, D. Fäh, N. Deichmann, and S. Sellami (2009). Probabilistic seismic hazard assessment of Switzerland: Best estimates and uncertainties, *J. Seismol.* **13,** 449–478.

Woessner, J., D. Laurentiu, D. Giardini, H. Crowley, F. Cotton, G. Grünthal, G. Valensise, R. Arvidsson, R. Basili, and M. B. Demircioglu (2015). The 2013 European seismic hazard model: Key components and results, *Bull. Earthq. Eng.* **13,** 3553–3596.

Worden, C., D. Wald, T. Allen, K. Lin, D. Garcia, and G. Cua (2010). A revised ground-motion and intensity interpolation scheme for ShakeMap, *Bull. Seismol. Soc. Am.* **100,** 3083–3096.

Zhao, J. X., J. Zhang, A. Asano, Y. Ohno, T. Oouchi, T. Takahashi, H. Ogawa, K. Irikura, H. K. Thio, P. G. Somerville, *et al.* (2006). Attenuation relations of strong ground motion in Japan using site classification based on predominant period, *Bull. Seismol. Soc. Am.* **96,** 898–913.

Department of Earth, Ocean and Ecological Sciences
University of Liverpool
Liverpool L69 3GP, United Kingdom
Ben.Edwards@liverpool.ac.uk
(B.E.)

Swiss Seismological Service (SED)
ETH Zürich
8092 Zürich, Switzerland
(C.C., L.D., D.F.)

Manuscript received 21 December 2015;
Published Online 5 July 2016